Energy Consumption Evaluation for Single-Source Vehicles

Apart from experimental tests, numeric simulation is a useful approach to estimate the energy consumption of single-source and hybrid-electric vehicles. After a brief introduction of simulation method for energy consumption evaluation, signal flows of quasi-static simulation are summarized for various types of vehicles. The analytic models developed in Chapter 2 are further validated at vehicle propulsion system level in terms of energy consumption.

3.1 Simulation Method

Numeric simulation is an efficient and effective method for the energy consumption evaluation. In general, two approaches are frequently applied to the energy consumption simulation: one is the quasi-static approach; and the other one is the dynamic approach.

3.1.1 Quasi-static Simulation

In quasi-static simulation, the energy consumption of a vehicle is estimated based on a given mission profile, efficiencies of the vehicle propulsion system depending on operating conditions, and parameters of vehicle features [42, 67]. The quasi-static simulation is performed in backward approach as sketched in Fig. 3.1.

Mission profile, including speed, road slope, etc., is discretized into many intervals by time step Δt. At each interval, variables of a mission profile are assumed to be constant.

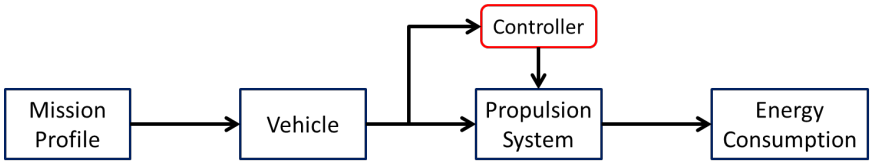

Figure 3.1 – Quasi-static simulation for energy consumption evaluation.

Then, vehicle load is estimated with vehicle parameters and mission variables through the load model in Chapter 2.6. Apart from the estimation of vehicle loads, kinetics of powertrain components are also evaluated with vehicle parameters (such as dynamic radius of tyre), mission variables, and powertrain parameters (for instance, final drive, transmission).

Next, vehicle load and kinetic variables are transmitted to the power source by the drivetrain. For example, vehicle load and speed of a conventional vehicle are transferred to the internal combustion engine in terms of torque and rotational speed, thus leading to the estimation of instantaneous fuel consumption. In contrast, vehicle load and speed in a battery-electric vehicle determine the torque and rotational speed of electric motor/generator, then these signals are used to evaluate voltage and current of battery. As a result, the instantaneous electrochemical power of battery is evaluated with previous proposed analytic models.

Finally, the instantaneous fuel consumption of the internal combustion engine or the electrochemical power of the battery are accumulated to the corresponding energy consumption. Energy consumption of conventional and hybrid-electric vehicles is measured by [L/hkm] (which is identical to [L/100km]); whereas, the metric for battery-electric vehicles is [kWh/km].

The quasi-static simulation is capable of the evaluation of energy consumption of advanced vehicle propulsion systems, particularly the minimum energy consumption of hybrid-electric vehicles. However, the physical causality cannot be respected due to the backward formulation.

3.1.2 Dynamic Simulation

Dynamic simulation is based on a mathematical description that represents the physical causality. The model is often formulated in forward approach using sets of ordinary differential equations in its state-space form to describe dynamic effects in a vehicle propulsion system.

Compared with quasi-static simulation, extra powertrain control systems and a

particular driver model are always required, as shown in Fig. 3.2. Powertrain control systems, such as engine control unit and transmission control unit, are lumped into the block of Controller. Because dynamic simulation is not implemented throughout this dissertation, this simulation method is not introduced in details. For example, a typical forward simulation tool ALPHA [68, 69] is available to the public.

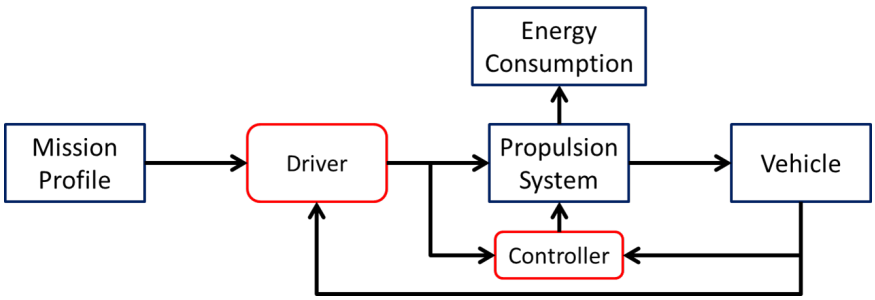

Figure 3.2 – Dynamic simulation for energy consumption evaluation.

3.2 Simulation Set-Up

Contributions of this thesis are based on quasi-static simulation method. Therefore, simulation set-ups are solely introduced for the quasi-static simulation in this section.

3.2.1 Mission Profile

Mission profile, also known as driving cycle, consists of historical trajectories of typical variables, and is an essential input to energy consumption evaluation for all categories of vehicles. Typical variables consist of speed and road slope (or, alternatively, altitude).

In general, mission profile includes two categories: the standardized driving cycles and the real-world driving cycles. Standardized driving cycles are used for regulation purpose. Energy consumption of a light-duty vehicle is certified by carrying out tests over a standardized driving cycle, such as the New European Driving Cycle (NEDC) in Fig. 3.3. As for real world driving cycles, they are recorded for specific purposes during experimental tests, for instance, a typical mission for urban delivery vans or trucks. More missions applied in this thesis are presented in Appendix C.2, which consists of Federal Test Procedure – 72 (FTP-72), HighWay Fuel Economy Test Cycle (HYWFET), Inner City Driving Cycle (ICDC) and Suburban Driving Cycle (SUDC). The main characteristics, including mean speed, distance, and maximal speed, are summarized in Appendix C.1.

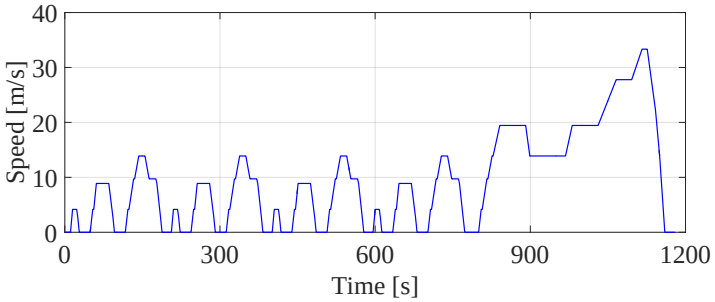

Figure 3.3 – Speed trajectory of NEDC.

Additionally, the trajectory of gear shift is required for vehicles equipped with manual transmissions. Gear shift schedules are usually provided in accordance with the standardized driving cycles. For example, the gear shift schedules, based on [70], for vehicles with five- or six-speed manual transmissions are depicted in Fig. 3.4.

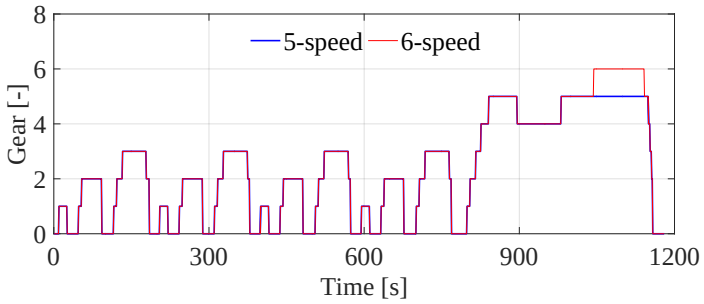

Figure 3.4 – Gear shift schedule over NEDC.

3.2.2 Signal Flow

Data in regard with mission profile, vehicle parameters, and vehicle propulsion system features is vital in quasi-static simulations. Variable flows and exchanges for conventional, battery-electric, and hybrid-electric vehicles, are summarized and sketched in terms of quasi-static simulations hereafter.

The evaluation of energy consumption for a conventional vehicle is completed through the quasi-static simulation illustrated in Fig. 3.5. A mission profile abbreviates to MP, whereas vehicle is shorten as VEH. The main powertrain components consist of internal combustion engine (ENG) and drivetrain (short for DRT), latter of which mainly contains a stepped-ratio transmission and final drive.

As shown in Fig. 3.5, vehicle speed v, acceleration a, and gear number n_t are provided by mission profiles. Then, the rotational speed of wheels (denoted by ω_w) and vehicle load in terms of torque (denoted by T_l) are evaluated with mission variables and vehicle parameters. Then, the wheel speed and vehicle load are transmitted by the drivetrain to the internal combustion engine. Thus, the output of drivetrain in terms of speed ω_d and torque T_d is identical to the input speed and torque (indicated by ω_e and T_e, respectively) to the internal combustion engine. Losses due to clutches or other coupling devices are not considered. Thanks to the determined engine speed and torque, the instantaneous power of burned fuel is converted from the fuel mass flow rate based on fuel consumption maps. Finally, the fuel consumption in [L/hkm] is computed over the test mission.

Figure 3.5 – Quasi-static simulation for conventional vehicles.

As the other type of single-source vehicles, battery-electric vehicles only consume electric energy stored in battery. The scheme of quasi-static simulation is depicted in Fig. 3.6 for the energy consumption evaluation of a battery-electric vehicle. Apart from mission profiles and vehicle parameters, the main powertrain components of a battery-electric vehicle consist of drivetrain (DRT), electric motor/generator (EMG), and battery (BAT). Currently, a simple drivetrain, including final drive and a single-speed transmission, is widely implemented to battery-electric vehicles.

Due to the implementation of simple gear-trains, variables of a mission profile only account for speed v and acceleration a. Then, vehicle load in terms of torque (T_l) and wheel speed (ω_w) are calculated using vehicle parameters. The output torque and speed of the drivetrain (indicated by T_d and ω_d) are directly transmitted to the electric motor/generator. Thus, the speed and torque of EMG (ω_m and T_m) are equal to the ones of drivetrain. After the electric power of EMG is determined by its speed and torque, the electric power P_{me} is provided by the battery. Thus, the terminal power of battery P_b is assumed to be the electric power of EMG. Finally, electrochemical power of battery P_{be} is estimated at each time step, and then used to evaluate the energy consumption over the test mission.

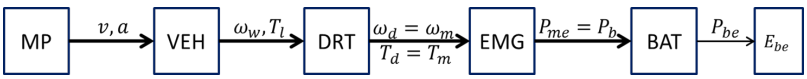

Figure 3.6 – Quasi-static simulation for battery-electric vehicles.

As for hybrid-electric vehicles, the energy consumption is evaluated through quasi-static simulations depending on powertrain architecture. In addition, an energy management strategy (Energy Management Strategy (EMS)) is requested to split the power between different energy sources.

Considering a series HEV, mission variables and vehicle parameters are similar to those of battery-electric vehicles. Compared with powertrain of a battery-electric vehicle, more powertrain components are installed in a series HEV, as illustrated in Fig. 3.7. The additional components consist of an electric generator (short for GEN) and an internal combustion engine (ENG).

Exchanges of variables and parameters are the same as in a battery-electric vehicle except for the involvement of EMS. The electric power of electric motor (MOT) P_{me} is satisfied by the terminal power of battery P_b and the electric power of generator P_{ge}. To minimize the energy consumption of internal combustion engine (E_{ef}), optimal control is required to determine control variable u. Throughout this thesis, control variable is always defined as $u(t) := P_b(t)$ for series HEVs, and the battery final state of energy is maintained the same as the initial one.

After the determination of control variable u, the power demand to battery (denoted by P_b) and to electric generator (indicated by P_{ge}) are used to evaluate the electrochemical power P_{be} and the power of burned fuel P_{ef}, respectively. Note that, the mechanical power of electric generator P_g is identical to the mechanical power of engine P_e.

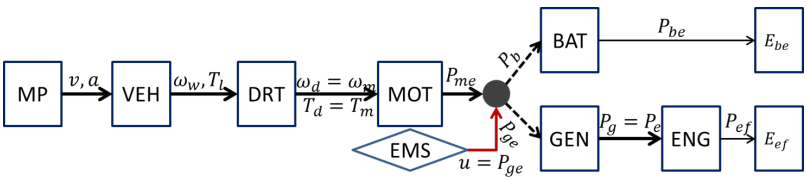

Figure 3.7 – Quasi-static simulation for series hybrid-electric vehicles.

The quasi-static simulation for parallel hybrid-electric vehicles is illustrated in Fig. 3.8, where the parallel HEV is of pre-transmission congratulation. Variables and parameters are transmitted in the same way as those are transferred in a conventional vehicle except for the involvement of EMS. The control variable is $u(t) := P_m(t)$ for parallel HEVs.

Thanks to the pre-transmission configuration, the speed from drivetrain (ω_d) is equal to the speed of engine (ω_e) and the one of electric motor (ω_m). Optimal control techniques are applied to determine the control variable in order to minimize the energy consumption of the internal combustion engine. With determined control variable, the

mechanical power of engine and motor (denoted by P_e and P_m, respectively) are used to compute the burned-fuel power P_{ef} and electrochemical power of battery P_{be}. Therefore, the energy consumption is evaluated based on the minimized fuel energy E_{ef}.

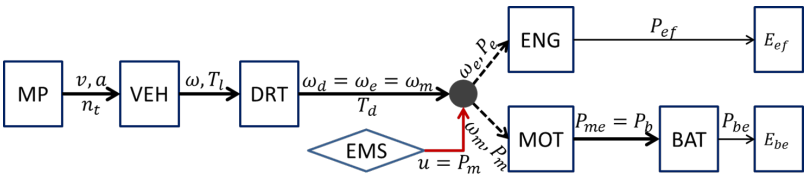

Figure 3.8 – Quasi-static simulation for parallel hybrid-electric vehicles.

To summarize, the quasi-static simulation in backward approach evaluates the instantaneous power based on the discretized variables of the investigated mission profile at each time step. In particular, the traditional optimal control is also realized based on the discretized control variable. Because of the quasi-static simulation, the approach for the energy consumption evaluation is designated as Quasi-Static Simulation (QSS).

3.3 Numeric Evaluation of Energy Consumption

In this section, energy consumption of single-source vehicles is evaluated through quasi-static simulation (QSS) based on different types of powertrain data. The categories of component data consist of grid-point data, description (estimated with the descriptive analytic models), and prediction (approximated with the descriptive analytic models). Energy consumption based on different types of powertrain data is compared, analysed, and discussed.

3.3.1 Conventional Vehicle

Reference Vehicle

Main features of the investigated conventional vehicle are summarized in Table 3.1, where the internal combustion engine and transmission are the engine ID1 and the dual clutch transmission ID14 in Table 2.5 and Table 2.7, respectively.

Results and Analysis

Results of energy consumption in terms of fuel consumption (FC) are depicted in Fig. 3.9 based on three standardized missions, which are NEDC, FTP-72, and HYWFET. The black bars represent the energy consumption evaluated with powertrain models

Vehicle	m_v [kg]	1595
	R_w [m]	0.308
	C_{v0} [N]	134.094
	C_{v1} [N/(m/s)]	3.746
	C_{v2} [N/(m/s)^2]	0.3486
Engine	$\mathcal{I}_e$	CI/TC
	$\mathcal{V}_e$ [L]	2.0
	$\mathcal{T}_e$ [Nm]	324
	$\mathcal{P}_e$ [kW]	98
Drivetrain	$\mathcal{I}_t$	DCT-6
	$\mathcal{R}_{fd}$	4.12 & 3.04

Table 3.1 – Features of investigated conventional vehicle.

of grid-point data; the blue bars indicate the evaluations based on descriptive analytic models of powertrain components; and the cyan bars show the evaluations based on predictive analytic models of powertrain components.

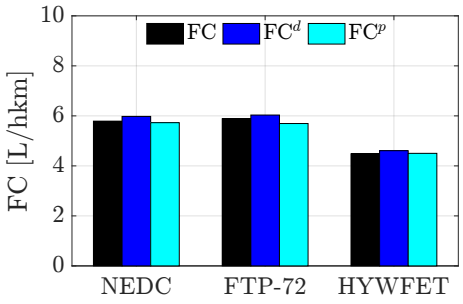

Figure 3.9 – Fuel consumption of reference conventional vehicle based on different types of powertrain component models.

In general, both descriptive and predictive analytic models of powertrain components can estimate energy consumption with high accuracy. The descriptive analytic models slightly overestimate the energy consumption over all mission profiles; whereas the predictive analytic models illustrate less errors than the descriptive analytic models over NEDC and HYWFET. The relative errors are quantified and summarized in Table 3.2 in terms of descriptive and predictive relative error (denoted correspondingly by ε^d and ε^p).

Mission Profile	ε^d [%]	ε^p [%]
NEDC	3.28	-1.05
FTP-72	2.53	-3.24
HYWFET	2.79	0.42

Table 3.2 – Descriptive and predictive errors of energy consumption with respect to grid-point data.

3.3.2 Battery-Electric Vehicle

Reference Vehicle

The investigated battery-electric vehicle is specified in Table 3.3, in which battery cells are of high energy ID4 and the electric motor/generator is PMSM ID7 in Table 2.11 and Table 2.14, respectively. The gear ratio of drivetrain is the combination of final drive and the motor gear ratio , which is computed by $\mathcal{R}_d = \mathcal{R}_m \mathcal{R}_{fd}$.

Vehicle	m_v [kg]	1318
	R_w [m]	0.287
	C_{v0} [N]	94.731
	C_{v1} [N/(m/s)]	5.931
	C_{v2} [N/(m/s)^2]	0.2865
Battery	$\mathcal{I}_b$	HE
	$\mathcal{Q}_b$ [Ah]	53
	$\mathcal{K}_b$	88
Electric Motor	$\mathcal{I}_m$	PMSM
	$\mathcal{T}_m$ [Nm]	108
	$\mathcal{P}_m$ [kW]	45
Drivetrain	$\mathcal{R}_d$	21

Table 3.3 – Features of investigated battery-electric vehicle.

Results and Analysis

Similar to the investigated conventional vehicle, energy consumption of the battery-electric vehicle are evaluated based on grid-point data, descriptive analytic models, and predictive analytic models of powertrain components. As two types of descriptive analytic models are developed for battery, results of energy consumption are presented into two groups, which are illustrated in Fig. 3.10a and 3.10b, respectively.

The quadratic analytic model of battery presents less errors in energy consumption

evaluation than the piece-wise linear analytic model does. Therefore, quadratic analytic model of battery is widely implemented in all types of electrified vehicle propulsion systems. In contrast, the piece-wise linear battery model is only applied in the fully-analytic energy consumption evaluation method for hybrid-electric vehicles, which aims to involve more powertrain dimensioning parameters as well as to reduce the complexity of combined analytic model of battery and electric motor/generator.

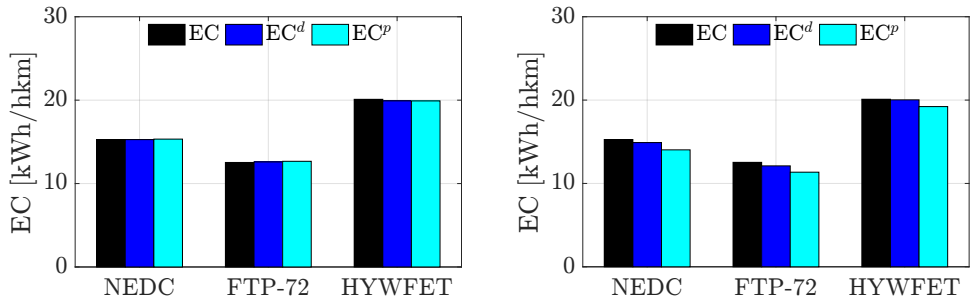

(a) quadratic battery model

(b) piece-wise linear battery model

Figure 3.10 – Energy consumption of reference battery-electric vehicle based on different types of powertrain component models.

Furthermore, relative errors of energy consumption of descriptive and predictive analytic models compared with those of grid-point data are listed in Table 3.4b and 3.4a correspondingly for the quadratic and piece-wise linear battery model. The quadratic battery model shows higher accuracy than the piece-wise linear model. As a result, the piece-wise linear battery model is used only in limited conditions where the quadratic battery model is no longer feasible.

Mission Profile	ε^d [%]	ε^p [%]
NEDC	0	0.39
FTP-72	0.56	1.12
HYWFET	-0.90	-0.95

(a) quadratic battery model

Mission Profile	ε^d [%]	ε^p [%]
NEDC	-2.42	-8.12
FTP-72	-3.35	-9.42
HYWFET	0.35	-4.38

(b) piece-wise linear battery model

Table 3.4 – Relative errors of energy consumption based on descriptive and predictive analytic models.

Chapter 4

Minimal Energy Consumption of Hybrid-Electric Vehicles

In this chapter, novel fast-running methods are proposed to estimate the minimal energy consumption of hybrid-electric vehicles, particularly series and parallel HEVs. Benchmarked by standard approaches of Pontryagin's Minimum Principle, the novel methods, Selective Hamiltonian Minimization (SHM) and GRaphical-Analysis-Based Energy Consumption Optimization (GRAB-ECO), significantly decrease the computation time of the evaluation of the minimum energy consumption for hybrid-electric vehicles.

4.1 Optimal Control Problem Formulation

Energy consumption is influenced by the powertrain control technique in a hybrid-electric vehicle. To benchmark the energy consumption in the early design stage, optimal control technique is applied to evaluate the minimum energy consumption. The optimal control problem of an HEV is formulated to minimize the objective function, which is

$$J(u(t)) = \int_{t_0}^{t_f} P_{ef}(u(t), t)dt, \tag{4.1}$$

where control variable $u(t)$ depends on powertrain architectures, which yields

$$u(t) = \begin{cases} P_b(t), & \text{series HEV,} \\ P_m(t), & \text{parallel HEV.} \end{cases} \tag{4.2}$$

Considering the system dynamics $\dot{x}$, it is independent from the system state and defined by

$$\dot{x}(t) = P_{be}(t). \tag{4.3}$$

The minimal energy consumption of an HEV is tailored for the charge-sustaining mode throughout this thesis. In other words, the final battery state of charge is $x(t_f) = x(t_0)$, thus leading to the varied electrochemical energy $\Delta E_{be}(t_f) = 0$.

According to Pontryagin's Minimum Principle and the independence of system state, the Hamiltonian function is expressed by

$$H(u(t), t) = P_{ef}(u(t), t) + s \cdot P_{be}(u(t), t), \tag{4.4}$$

where s is the adjoint state variable.

Within the full control space U in-between the bottom and top boundaries of the control variable, optimal control laws $u^*(t)$ are determined by finding

$$u^*(t) = \arg\min_{u \in U} H(u(t), s^*, t), \tag{4.5}$$

where the proper adjoint state variable s^* is evaluated based on the final state of charge requirement, which yields

$$\Delta E_{be}(t_f, s^*) = 0. \tag{4.6}$$

The constraints in the optimal control problem consist of singularity, equality and in-equality conditions due to powertrain limitations and models. Depending on the hybrid architecture, the equality constraint refers to the "power balance" yielding

$$\begin{cases} P_{ge}(t) + P_b(t) = P_{me}(t), & \text{series HEV}, \\ P_m(t) + P_e(t) = P_d(t), & \text{parallel HEV}, \end{cases} \tag{4.7}$$

where P_{me} is the electric power of traction motor satisfied by battery terminal power P_b and electric power of generator P_{ge}; P_d is the power demand of drivetrain satisfied by engine brake power P_e and mechanical power of electric motor P_m.

Concerning the inequality constraints, they originate from the physical limits of the powertrain components and the operating limits, such as the boundaries of battery

terminal power. However, the constraint of instantaneous battery state of charge is not considered throughout this thesis.

4.2 Fully Numeric Solution

Based on PMP, Hybrid Optimization Tool (HOT) [71] and Vectorized Hybrid Optimization Tool (VHOT) [72] are simulation tools of iterative and vectorized approach, respectively. As standard approaches, both HOT and VHOT benchmark the performance of novel fast-running methods in Section 4.3 and 4.4.

Because HOT and VHOT are not the main outcomes of this thesis, the basic ideas and characteristics are briefly summarized for introduction. In both HOT and VHOT, the control variable $u(t)$ at each time step is quantified as

$$u_k(t) = u_0(t) + k\Delta u, \quad (k = 0, 1, \cdots, n_u), \tag{4.8}$$

where u_0 is the minimal admissible value of control variable $u(t)$, Δu is the control variable step, and n_u is the resolution of discretization. According to the power balance in Eq. 4.7, the Hamiltonian function in Eq. 4.4 is evaluated for each discretized control variable $u_k(t)$ at each time step.

The main difference between HOT and VHOT is the minimization process. The minimal energy consumption is evaluated through iterative processes in HOT as shown in Fig. 4.1a, whereas the minimization of energy consumption is performed through the array operation in VHOT as depicted in Fig. 4.1b. HOT needs three loops to evaluate the minimum energy consumption, which complete a specific mission, find optimal control laws, and determine proper adjoint state variable. The discrepancy of the final state of the control system is taken into account by the equivalent fuel consumption model in Chapter 6.2.2. In contrast, VHOT minimizes the energy consumption based on array operation. The final battery state of charge is maintained to be the same as the desired value, thereby leading to the estimation of the proper adjoint state variable by numeric interpolation. Thanks to the substitution of iteration with array operation, VHOT takes much less computation time than HOT does. Relevant results are found in Section 4.5.

In the flow charts of HOT and VHOT in Fig 4.1, variable $\mathcal{C}$ denotes the cycle-related variables (such as speed, acceleration); whereas $\mathcal{D}$ indicates the dimension-related parameters (including dimensioning parameters of powertrain components and vehicle parameters). Variable $V(t, u, s)$ represents generic variables along dimensions of time t, control u, and adjoint variable s.

As a solution of LMS Imagine.Lab Amesim, HOT is introduced with details in [65, 71, 73]. The improved version VHOT is specifically reported in [72].

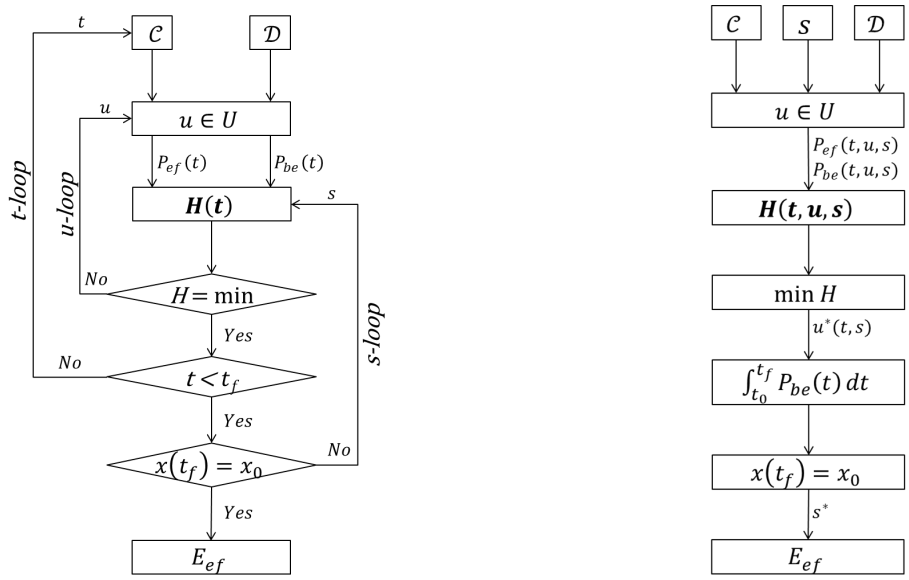

(a) HOT (b) VHOT

Figure 4.1 – Flow chart of PMP-based standard approaches.

4.3 Semi-Analytic Solution

A novel semi-analytic method is proposed to estimate the minimal energy consumption for series or parallel hybrid-electric vehicles, which takes less computation time than both HOT and VHOT. Thanks to analytic models of powertrain components, the Hamiltonian function is formulated in closed form in the novel method. Therefore, solution to the minimization of Hamiltonian is derived analytically. Due to further limited possible optimal control cases (denoted by $U_i (i = 1, 2, \cdots)$) in the full control space, this method is designated as Selective Hamiltonian Minimization (SHM).

The flow chart of SHM is illustrate in Fig. 4.2. Compared with the full quantification of control variable in HOT and VHOT, SHM reduces its full control space into limited number of cases. In details, five ($i = 5$) cases are considered for series HEVs; whereas six ($i = 6$) cases exist for parallel HEVs. Except for the dimension reduction of the full control space, the procedure and operation of SHM is the same as that of VHOT. Therefore, SHM can be concluded as an analytic version of VHOT.

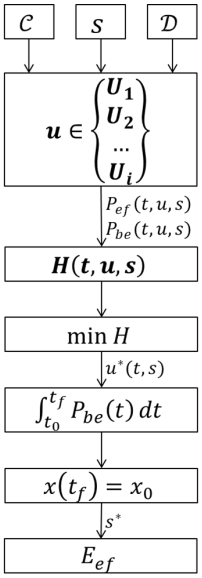

Figure 4.2 – Flow chart of SHM.

4.3.1 Series Hybrid-Electric Vehicle

Analytically solvable Hamiltonian is formulated based on analytic models of powertrain components and vehicle load given in Chapter 2. However, the Hamiltonian function cannot be formulated in closed form due to the operation of the internal combustion engine and electric generator.

Auxiliary Power Unit

In series HEVs, the auxiliary power unit is a combination of internal combustion engine and electric generator. Due to the engine speed is independent from the wheel speed, the operating condition of an Auxiliary Power Unit (APU) is totally independent from the vehicle operating condition. To simplify the operation of an APU, it is managed to follow the Optimal Operating Line (OOL), which represents the best operating efficiency. Therefore, the analytic model required to formulate the closed form Hamiltonian is given by

$$P_{ef}(P_{ge}) = k_{u0} + k_{u1}P_{ge} + k_{u2}P_{ge}^2, \tag{4.9}$$

where coefficients $k_{ui}(i = 0, 1, 2)$ are numerically identified from either the descriptive or the predictive analytic models of internal combustion engines and electric generators.

Hamiltonian Function

According to the power balance in Eq. 4.7, the electric power of an APU is calculated by

$$P_{ge}(t) = P_{me}(t) - P_b(t). \tag{4.10}$$

Combining Eq. 4.9 and 4.10, Hamiltonian in Eq. 4.4 is rewritten as

$$H(t,u,s) = k_{h0} + k_{h1}(s)P_b(t) + k_{h2}(s)P_b^2(t), \tag{4.11}$$

where the control variable is $u := P_b(t)$, and parameters $k_{hi}(i = 0,1,2)$ are expressed as

$$k_{h0}(t,s) = k_{u0} + k_{u1}P_{me}(t) + k_{u2}P_{ge}^2(t) + sk_{b0}, \tag{4.12}$$

$$k_{h1}(t,s) = sk_{b1} - k_{u1} - 2k_{u2}P_{me}(t), \tag{4.13}$$

$$k_{h2}(s) = sk_{b2} + k_{u2}. \tag{4.14}$$

Due to physical limits, the operating constraints of battery are summarized as

$$P_b(t) \in \left[\underline{P}_b,\ \overline{P}_b\right]. \tag{4.15}$$

Taking the physical limits of APU ($P_{ge}(t) \in [0, \overline{P}_{ge}]$) and the power balance in Eq. 4.10 into account, another operating constraint of battery is derived as

$$P_b(t) \in \left[P_{me}(t) - \overline{P}_{ge},\ P_{me}(t)\right]. \tag{4.16}$$

Minimization of Hamiltonian

The unconstrained solution to the minimization of Hamiltonian is derived from $\dfrac{\partial H}{\partial u} = 0$ $\left(\ u = P_b(t)\ \right)$, which yields

$$P_{b,unc}(t,s) = \frac{k_{u1} + 2k_{u2}P_{me}(t) - sk_{b1}}{2\left(sk_{b2} + k_{u2}\right)}. \tag{4.17}$$

Considering the possible constrained solutions resulting from the physical and operating limits of powertrain components, the constrained possible solutions to the minimization of Hamiltonian are expressed by

$$P_{b,c1}(t) = P_{me}(t), \tag{4.18}$$

$$P_{b,c2}(t) = P_{me}(t) - \overline{P}_{ge}, \tag{4.19}$$

$$P_{b,c3}(t) = \overline{P}_b, \tag{4.20}$$

$$P_{b,c4}(t) = \underline{P}_b. \tag{4.21}$$

Considering $U_1 := P_{b,unc}(t,s)$, $U_2 := P_{b,c1}(t)$, $U_3 := P_{b,c2}(t)$, $U_4 := P_{b,c3}(t)$, $U_5 := P_{b,c4}(t)$, the full control space U for series hybrid-electric vehicles is defined by

$$u \in \Big\{U_1, U_2, \cdots, U_5\Big\}. \tag{4.22}$$

4.3.2 Parallel Hybrid-Electric Vehicle

Being comparable to APU, the Electric Drive Unit (EDU) is applied in parallel hybrid-electric vehicles to formulate the closed-form Hamiltonian function so that it can be solved analytically. The EDU is a combination of the battery and electric motor, which both have quadratic analytic models. To formulate the closed-form Hamiltonian function, an analytic model of EDU must be derived.

Electric Drive Unit

Considering the analytic model of battery in Eq. 2.30 and the one of electric motor/-generator in Eq. 2.35, the electrochemical power of an EDU is analytically modeled by

$$P_{be}(P_m, \omega_m) = k_{u0}(\omega_m) + k_{u1}(\omega_m)P_m(\omega_m) + k_{u2}(\omega_m)P_m^2(\omega_m), \tag{4.23}$$

where the coefficients $k_{ui}(i = 0, 1, 2)$ are numerically identified from either the grid-point data, description, or prediction of batteries and electric motor/generators. Note that, the quadratic analytic model of battery is applied for better accuracy.

Hamiltonian Function

According to the power balance in Eq. 4.7, the engine power is calculated by

$$P_e(t) = P_d(t) - P_m(t). \tag{4.24}$$

Combining Eq. 4.23 and 4.24, the Hamiltonian function in Eq. 4.4 is re-written by

$$H(t,u,s) = k_{h0}(t,s) + k_{h1}(t,s)P_m(t) + k_{h2}(t,s)P_m^2(t), \tag{4.25}$$

where the control variable is $u := P_m(t)$. The parameters $k_{hi}(i = 0, 1, 2)$ are

$$k_{h0}(t,s) = k_{e0}(t) + k_{e1}(t)P_d(t) + k_{e2}(t)P_d^2(t) + sk_{u0}(t), \tag{4.26}$$

$$k_{h1}(t,s) = sk_{u1}(t) - k_{e1}(t) - 2k_{e2}(t)P_d(t), \tag{4.27}$$

$$k_{h2}(t,s) = sk_{u2}(t) + k_{e2}(t), \tag{4.28}$$

where parameter k_{e2} is null when light-duty engines are applied.

As given by Eq.4.25, the closed-form Hamiltonian is formulated as a quadratic function of control variable P_m, despite the piece-wise linear model for light-duty engines in Eq.2.2. In fact, only the first case of the piece-wise linear model is considered, because the complete range of engine efficiency has been fully considered in this case. To remind that engine corner power P_{ec} represents the best efficiency of an engine.

Considering the physical limits, the constraints of electric motor/generator are given by

$$P_m(t) \in \left[\underline{P}_m(t),\ \overline{P}_m(t)\right]. \tag{4.29}$$

In addition, the physical limits of internal combustion engine $\left(P_e(t) \in [0, \overline{P}_e(t)]\right)$ and the power balance in Eq. 4.24 result a second constraint, which is

$$P_m(t) \in \left[P_d(t) - \overline{P}_e(t),\ P_d(t)\right]. \tag{4.30}$$

Apart from operating constraints, an extra discontinuity in Eq. 2.2 is considered that leads to the mechanical power of electric motor

$$P_m(t) = P_d(t) - P_{ec}(t). \tag{4.31}$$

Minimization of Hamiltonian

The unconstrained solution to the Hamiltonian minimization is derived by $\frac{\partial H}{\partial u} = 0$ $\Big($ $u = P_m(t)$ $\Big)$, which yields

$$P_{m,unc}(t,s) = \frac{k_{e1}(t) + 2k_{e2}(t)P_d(t) - sk_{u1}(t)}{2\left(sk_{u2}(t) + k_{e2}(t)\right)}. \tag{4.32}$$

The possible constrained solutions resulting from the operating constraints of pow-

ertrain components are expressed as

$$P_{m,c1} = P_d(t), \tag{4.33}$$

$$P_{m,c2} = P_d(t) - \overline{P}_e(t), \tag{4.34}$$

$$P_{m,c3} = \overline{P}_m(t), \tag{4.35}$$

$$P_{m,c4} = \underline{P}_m(t). \tag{4.36}$$

As for the discontinuous solution, it is written by

$$P_{m,s1} = P_d(t) - P_{ec}(t). \tag{4.37}$$

Considering $U_1 := P_{m,unc}(t,s)$, $U_2 := P_{m,c1}(t)$, $U_3 := P_{m,s1}(t)$, $U_4 := P_{m,c3}(t)$, $U_5 := P_{m,c4}(t)$, $U_6 := P_{m,c2}(t)$, the full control space U for parallel hybrid-electric vehicles is defined by

$$u \in \left\{U_1, U_2, \cdots, U_6\right\}. \tag{4.38}$$

4.3.3 Summary

One unconstrained solution and a limited number of constrained and discontinuous solutions owing to operating limits and discontinuity of analytic models constitute the full control space U of the Selective Hamiltonian Minimization (SHM). The computation time of SHM benefits from the decreased dimensions of the full control space U.

Compared with HOT and VHOT, SHM is characterized by an analytic solution of the Hamiltonian function. Although the engine on/off signal is not handled explicitly in the minimization of Hamiltonian, the corresponding case of engine off exists in the full control space. However, analytic method cannot find a suitable adjoint state variable s^* such that the varied electrochemical energy of battery meets the requirement.

Furthermore, it is impossible to evaluate the energy consumption through a closed-form solution along the time dimension. In other words, SHM evaluates the minimal energy consumption step by step along the time dimension. The procedure and operation of energy consumption minimization of SHM is the same as VHOT.

4.4 Approximate Solution

It is always not enough to reduce the computation time of minimal energy consumption estimation for hybrid-electric vehicles as the optimal design of vehicle propulsion

systems is always time-consuming. An extreme fast-running sub-optimal method, GRAB-ECO, is proposed to approximate the minimal energy consumption for series and parallel HEVs.

4.4.1 Fundamentals of GRAB-ECO

GRAB-ECO, standing for GRaphical-Analysis-Based Energy Consumption Optimization, approximates the minimal energy consumption by maximizing the average operating efficiency of the primary energy source, which has the worst efficiency. The primary energy source is the auxiliary power unit in a series HEV, and the internal combustion engine in a parallel HEV.

The working flow of GRAB-ECO is summarized and sketched in Fig. 4.3. The GRAB-ECO is characterized by a best-efficiency indicator $I_e(t)$, permutation of variables $I_e(\tau)$, and limited operating modes.

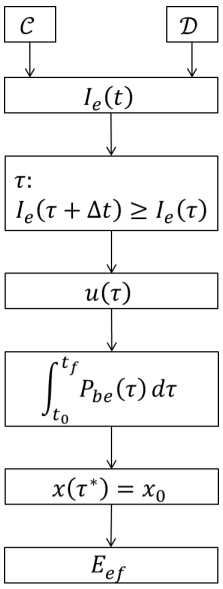

Figure 4.3 – Flow chart of GRAB-ECO.

The best-efficiency indicator evaluates the ratio between the demanded power to the power of the best efficiency of the primary energy source (e.g. APU in series hybrid-electric vehicles, and engine in parallel hybrid-electric vehicles) as well as determines the operating mode at each time step.

In regard with operating modes over a given mission, they consist of the **electric vehicle operation** and **hybrid vehicle operation**. In each operating mode, two sub-modes are categorized in terms of the **fixed mode** and **flexible mode**. Therefore, the

four operating modes are the *fixed electric vehicle mode* (*ev0*), the *flexible electric vehicle mode* (*ev1*), the *fixed hybrid vehicle mode*, and the *flexible hybrid vehicle mode* (*hv1*). A mathematical definition of these four operating modes will be found in Step 2 in the following section.

4.4.2 Essential Steps of GRAB-ECO

GRAB-ECO consists of four essential steps: the evaluation of best-efficiency indicator, the determination of instantaneous operating mode, the approximation of battery state of charge, and the estimation of minimal energy consumption.

Step 1: Indicator Evaluation

An indicator evaluates the distance between the power demand and the best-efficiency operating condition of the primary power source. Thus, this indicator is designated as the best-efficiency indicator. The higher the best-efficiency indicator, the greater the opportunity to shift the operation of the primary energy source to the best-efficiency point. On the other hand, the lower the best-efficiency indicator, the higher the opportunity to eliminate the operation of the primary energy source. In the unconstrained condition, the best-efficiency indicator I_e is evaluated by

$$I_e(t) = \begin{cases} \dfrac{P_{me}(t)}{P_{apu}}, & \text{series HEV,} \\ \dfrac{P_d(t)}{P_{ec}(t)}, & \text{parallel HEV,} \end{cases} \tag{4.39}$$

where P_{apu} is the absolute electrical power of the best-efficiency operating point of APU, P_{me} the power demand of the electric motor in a series HEV, P_d is the power demand of the drivetrain in a parallel HEV, and P_{ec} is the corner power of an internal combustion engine.

When the indicator $I_e(t) = 0$, the primary energy source does not provide any power. In other words, an HEV could be in standstill condition or in pure battery electric vehicle operating condition. When the indicator $I_e(t) = 1$, the primary energy source is working at its best efficiency regardless of the battery operating conditions. An example of the unconstrained best-efficiency indicator I_e is illustrated in Fig. 4.4 for a parallel HEV. The power of drivetrain estimated over NEDC is presented as well.

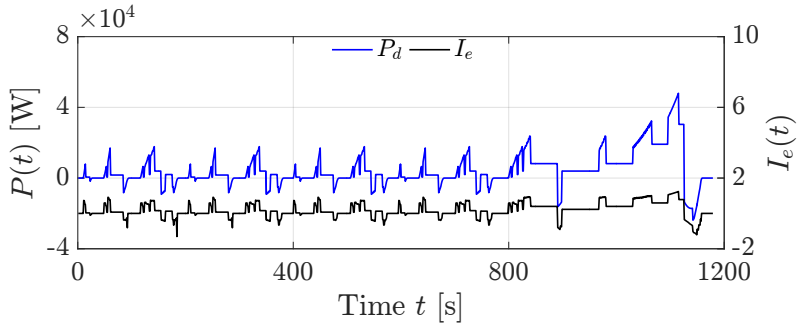

Figure 4.4 – Example of best-efficient indicator and power of drivetrain over NEDC.

Step 2: Mode Determination

To explicitly determine the vehicle operating mode, a sorted best-efficiency indicator $I_e(\tau)$ is obtained according to a new time series τ. The new time series τ is the permutation of time t, such that

$$I_e(\tau + \Delta t) \geq I_e(\tau), \forall \tau \in [t_0, t_f], \tag{4.40}$$

where Δt is the time step, t_0 and t_f correspond to the first and last time step of the investigated mission. For example, a mapping between the actual discrete time index (denoted by t) and the sorted index (denoted by τ) is illustrated in Fig. 4.5.

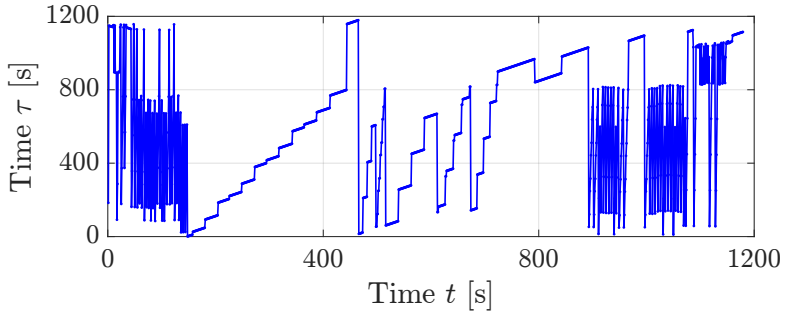

Figure 4.5 – Example of mapping between actual and sorted time index over NEDC.

Based on the sorted best-efficiency indicator $I_e(\tau)$ over time series τ (see Fig. 4.6), operating constraints of powertrain components are sorted and then considered to determine vehicle operating modes. The basic idea to cope with the operating constraints is to maximize the instantaneous operating efficiency of the primary energy source at

each time interval either by eliminating the engine operation or by implementing the maximal efficiency of the primary energy source. An example of the implementation of constraints is reported in [60].

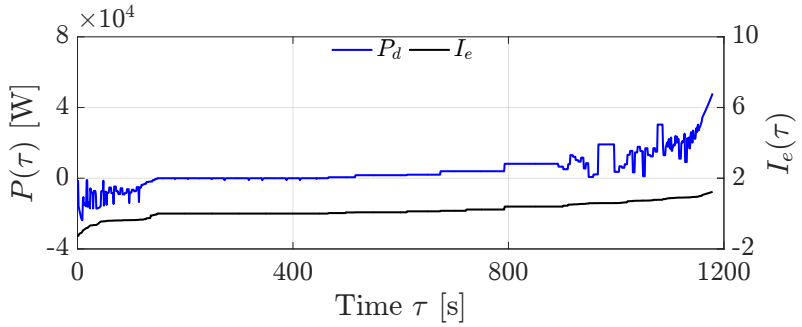

Figure 4.6 – Example of sorted variables over NEDC.

The operating modes of a series HEV and of a parallel HEV are correspondingly determined by

$$u(\tau) := P_b(\tau) = \begin{cases} P_{me}(\tau), & \tau \in [\tau_0, \tau_1], \\ P_{me}(\tau), & \tau \in (\tau_1, \tau^*], \\ P_{me}(\tau) - P_{apu}(\tau), & \tau \in (\tau^*, \tau_2), \\ P_{me}(\tau) - P_{apu}(\tau), & \tau \in [\tau_2, \tau_f], \end{cases} \tag{4.41}$$

and

$$u(\tau) := P_m(\tau) = \begin{cases} P_d(\tau), & \tau \in [\tau_0, \tau_1], \\ P_d(\tau), & \tau \in (\tau_1, \tau^*], \\ P_d(\tau) - P_{ec}(\tau), & \tau \in (\tau^*, \tau_2), \\ P_d(\tau) - P_{ec}(\tau), & \tau \in [\tau_2, \tau_f]. \end{cases} \tag{4.42}$$

As shown in Fig. 4.7, the determination of the operating mode of a parallel HEV is exemplified. The green area refers to the operating mode *ev0*, when time $\tau \in [\tau_0, \tau_1]$; the cyan area represents the operating mode *ev1*, when time $\tau \in (\tau_1, \tau^*]$; the magenta area indicates the operating mode *hv1*, while time $\tau \in (\tau^*, \tau_2)$; and, the red area is the operating mode *hv0*, while time $\tau \in [\tau_2, \tau_f]$.

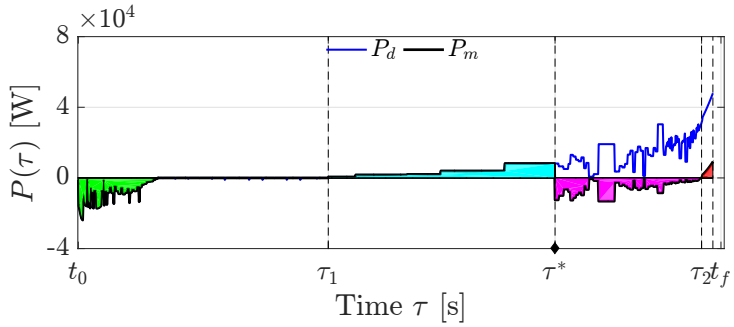

Figure 4.7 – Operating mode determination of GRAB-ECO for parallel HEVs.

The time instant τ_1 and τ_2 are correspondingly defined by

$$\{\tau_1 : I_e(\tau_1) \leq 0 \cap I_e(\tau_1 + \Delta t) > 0\}, \tag{4.43}$$

$$\{\tau_2 : I_e(\tau_2) < 1 \cap I_e(\tau_2 + \Delta t) \geq 1\}. \tag{4.44}$$

As for the time instant τ^*, it is an essential time instant that is introduced in the following step.

Step 3: State Approximation

According to the operating modes determined in the previous step, the resulting electrochemical energy of the battery in each operating mode is calculated by

$$E_{be,ev0} = \sum_{\tau=\tau_0}^{\tau_1} \Psi(u_{ev0}(\tau))\Delta t, \tag{4.45}$$

$$E_{be,hv0} = \sum_{\tau=\tau_2}^{\tau_f} \Psi(u_{hv0}(\tau))\Delta t, \tag{4.46}$$

$$E_{be,ev1}(\tau^*) = \sum_{\tau=\tau_1}^{\tau^*} \Psi(u_{ev1}(\tau))\Delta t, \tag{4.47}$$

$$E_{be,hv1}(\tau^*) = \sum_{\tau=\tau^*}^{\tau_2} \Psi(u_{hv1}(\tau))\Delta t, \tag{4.48}$$

where Ψ represents the generic function that evaluates the electrochemical power of battery of a given HEV.

The essential time instant τ^*, affected by the requirement of the final state of charge of

the battery, is found in-between the instant τ_1 and τ_2. As a result, the flexible operating modes *ev1* and *hv1* are segmented by the time instant τ^* that is evaluated using the algorithm of root–finding in terms of interpolation. In other words, the turning point τ^* is a time instant such that

$$\Delta E_{be}(\tau^*) = 0, \tag{4.49}$$

where the varied electrochemical energy of battery is calculated by

$$\Delta E_{be}(\tau^*) = E_{be,ev0} + E_{be,hv0} + E_{be,ev1}(\tau^*) + E_{be,hv1}(\tau^*). \tag{4.50}$$

Fig. 4.8 presents the resulting electrochemical energy of battery in each operating mode. The varied electrochemical energy ΔE_{be} is depicted as a function of time τ. Numeric interpolation is used to evaluate the essential time instant τ^* marked with a black bullet.

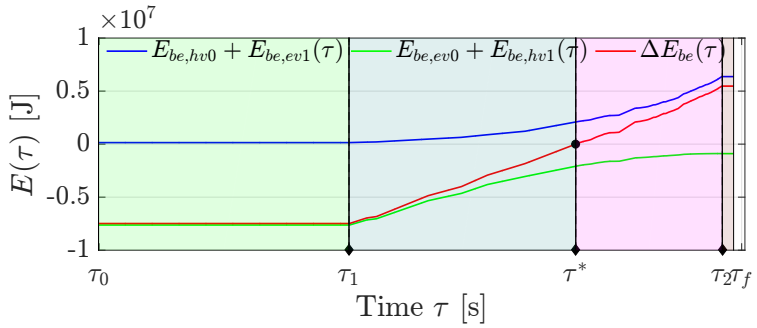

Figure 4.8 – Resulting electrochemical energy of battery in accordance with the operating modes.

Step 4: Energy Estimation

As a consequence of the essential time instant determination, the control variable of a series HEV is simplified as

$$u(\tau) = \begin{cases} P_{me}(\tau), & \tau \le \tau^*, \\ P_{me}(\tau) - P_{apu}(\tau), & \tau > \tau^*, \end{cases} \tag{4.51}$$

whereas the control variable of a parallel HEV is

$$u(\tau) = \begin{cases} P_d(\tau), & \tau \leq \tau^*, \\ P_d(\tau) - P_{ec}(\tau), & \tau > \tau^*. \end{cases} \tag{4.52}$$

Consequently, the minimal energy consumption of an HEV in terms of series or parallel architecture is approximated by

$$E_{ef} = \sum_{\tau=\tau^*}^{\tau_f} \Phi(u^*(\tau))\Delta t, \tag{4.53}$$

where Φ represents the generic function to evaluate the burned fuel power for an HEV.

4.4.3 Summary

GRAB-ECO approximates the minimal energy consumption of HEVs based on the maximization of average operating efficiency of the primary energy source. Compared with SHM, GRAB-ECO further decreases the control space U to only two operating conditions (electric and hybrid condition). Consequently, GRAB-ECO has the potential to further reduce the computation time compared with SHM. The results will be found in the following section.

4.5 Evaluation of Minimal Energy Consumption

In this section, minimal energy consumption of hybrid-electric vehicles is evaluated through QSS based on different types of powertrain component models, which consist of grid-point data, description (estimated with the descriptive analytic models), and prediction (approximated with the descriptive analytic models).

For each kind of powertrain component models, various methods are applied to evaluate the minimal energy consumption, including SHM, GRAB-ECO, HOT and VHOT. The performance of SHM and GRAB-ECO is benchmarked by HOT and VHOT in terms of fuel consumption and computation time. The corresponding computation time is the average value of twenty repetitions in terms of CPU time. Evaluations of minimum energy consumption are performed in MATLAB R2015b on a i7–4810QM CPU @ 2.80 GHz machine with 16 GB RAM.

Results of the minimum energy consumption as well as the average computation time of the investigated hybrid-electric vehicles are comparatively illustrated over various

investigated missions. Considering the evaluation based on HOT, the error of the final state of charge is compensated by the equivalent fuel consumption model introduced in Chapter 6.2.2; whereas the proper adjoint state variable s is found by the root-finding algorithm of Newton's method. The discretization step the adjoin variable s in VHOT is maintained the same as in SHM. As for the discretization step of time is always one second for all investigated methods.

4.5.1 Series Hybrid-Electric Vehicle

Reference Vehicle

Main features of the investigated series HEV are summarized in Table 4.1, where the internal combustion engine, electric generator, battery, and electric motor correspond to ENG ID7 in Table 2.5, PMSM ID6 in Table 2.14, BAT ID4 in Table 2.11, and PMSM ID11 in Table 2.14.

Vehicle	m_v [kg]	1648
	R_w [m]	0.308
	C_{v0} [N]	152.383
	C_{v1} [N/(m/s)]	1.346
	C_{v2} [N/(m/s)^2]	0.3751
Engine	$\mathcal{I}_e$	CI/TC
	$\mathcal{V}_e$ [L]	1.2
	$\mathcal{T}_e$ [Nm]	145
	$\mathcal{P}_e$ [kW]	43
Electric Generator	$\mathcal{I}_g$	PMSM
	$\mathcal{T}_g$ [Nm]	72
	$\mathcal{P}_g$ [kW]	30
Battery	$\mathcal{I}_b$	HE
	$\mathcal{Q}_b$ [Ah]	53
	$\mathcal{K}_b$	96
Electric Motor	$\mathcal{I}_m$	PMSM
	$\mathcal{T}_m$ [Nm]	108
	$\mathcal{P}_m$ [kW]	45
Drivetrain	$\mathcal{R}_d$	9.7

Table 4.1 – Main features of investigated series hybrid-electric vehicle.

Results and Analysis

Fig. 4.9 shows minimal energy consumption in terms of fuel consumption evaluated through various minimization methods over NEDC. Moreover, the minimal fuel consumption is estimated based on different types of powertrain component models. The black, blue, and cyan bars correspondingly indicate the evaluation based on grid-point data, descriptive analytic models, and predictive ones.

The main errors were caused by the powertrain component models (in terms of grid-point data, descriptive analytic models, and predictive models). This was always true to all of the minimization methods including HOT, VHOT, SHM, and GRAB-ECO. However, the discrepancies among the energy consumption evaluated based on the same type of powertrain component model but different minimization methods are not so significant as the typology of powertrain component models.

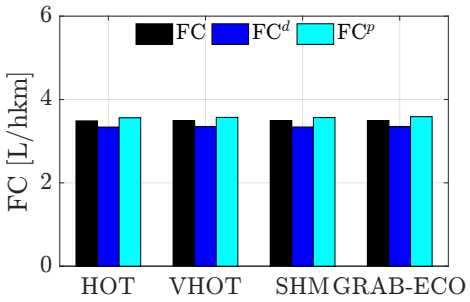

Figure 4.9 – Minimal energy consumption of reference series HEV over NEDC.

In addition, the exact errors of minimal energy consumption between grid-point data and descriptive analytic models and between grid-point data and predictive analytic models are listed in Table 4.2. In summary, the predictive analytic models of powertrain components are able to evaluate the minimal energy consumption of series HEVs through the proposed minimization methods in this chapter.

	HOT	VHOT	SHM	GRAB-ECO
ε^d [%]	-4.26	-4.07	-4.43	-4.19
ε^p [%]	2.13	2.26	2.06	2.69

Table 4.2 – Relative errors of minimal fuel consumption over NEDC.

The average computation time is summarized in Table 4.3 in terms of CPU time in [s]. The CPU time is the mean value of the computation time of twenty repetitions. Computation time is denoted by t_c^g, t_c^d, and t_c^p corresponding to the average time asso-

ciated with grid-point data, descriptive, and predictive analytic models. Specifically, SHM minimized energy consumption within tens of milliseconds, which was about ten times less than that of VHOT. Moreover, GRAB-ECO took seven to twelve milliseconds, which was about six times less than that of SHM.

The analytic models either at descriptive level or at predictive level shortened the computation time compared with the grid-point data. Significant computation time abatement was achieved by GRAB-ECO that shrunk the dimension of full control space . Therefore, the smaller dimension of the full control space results in the less computation time of minimal energy consumption evaluation.

	HOT	VHOT	SHM	GRAB-ECO
t_c^g [s]	963.93	0.4607	0.0916	0.0124
t_c^d [s]	838.11	0.5302	0.0412	0.0070
t_c^p [s]	675.69	0.4379	0.0410	0.0069

Table 4.3 – Comparison of average computation time over NEDC.

Apart from NEDC, the reference series HEV is also investigated over FTP-72 and HYWFET. Results of energy consumption over FTP-72 and HYWFET are correspondingly illustrated in Fig. 4.10a and 4.10b. Observations of the minimal energy consumption over NEDC were also true to those over FTP-72 and HYWFET.

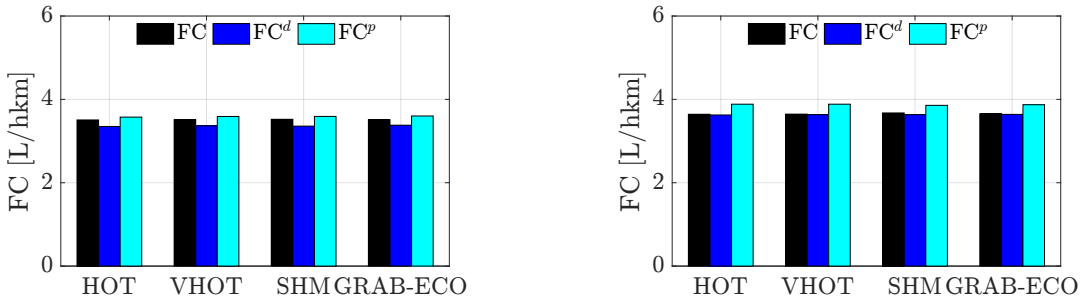

(a) FTP–72

(b) HYWFET

Figure 4.10 – Minimal energy consumption of reference series HEV over FTP-72 and HYWFET.

The relative errors of minimal energy consumption are summarized in Table 4.4 and 4.5 for FTP-72 and HYWFET, respectively. The discrepancies of minimal energy consumption between grid-point data and of predictive analytic models were higher over HYWFET. In addition, the minimal energy consumption was significantly overestimated

with powertrain models of predictive analytic models over HYWFET, compared with other missions.

	HOT	VHOT	SHM	GRAB-ECO
ε^d [%]	-4.46	-4.14	-4.66	-3.75
ε^p [%]	1.94	2.29	1.96	2.55

Table 4.4 – Relative errors of minimal fuel consumption over FTP-72.

	HOT	VHOT	SHM	GRAB-ECO
ε^d [%]	-0.45	-0.34	-1.12	-0.32
ε^p [%]	6.65	6.55	4.96	6.03

Table 4.5 – Relative errors of minimal fuel consumption over HYWFET.

As for average computation time of each evaluation, they are listed in Table 4.6 and 4.7 for FTP-72 and HYWFET, respectively. Apart from the significant abatement of computation time by SHM and GRAB-ECO, the average computation time also associated with the duration of missions. However, the average computation time of GRAB-ECO seemed not to be affected by the duration of missions.

	HOT	VHOT	SHM	GRAB-ECO
t_c^g [s]	1246.95	0.48280	0.10300	0.0128
t_c^d [s]	915.02	0.74540	0.04740	0.0073
t_c^p [s]	988.95	0.67450	0.04740	0.0071

Table 4.6 – Comparison of average computation time over FTP-72.

	HOT	VHOT	SHM	GRAB-ECO
t_c^g [s]	700.89	0.2943	0.0536	0.0121
t_c^d [s]	538.21	0.6169	0.0333	0.0076
t_c^p [s]	538.98	0.3308	0.0270	0.0068

Table 4.7 – Comparison of average computation time over HYWFET.

4.5.2 Parallel Hybrid-Electric Vehicle

Reference Vehicle

Main features of the investigated parallel HEV are summarized in Table 4.8, where battery is BAT ID1 in Table 2.11, and electric motor is PMSM ID5 in Table 2.14.

Vehicle	m_v [kg]	1814
	R_w [m]	0.317
	C_{v0} [N]	93.5
	C_{v1} [N/(m/s)]	5.29
	C_{v2} [N/(m/s)^2]	0.536
Engine	$\mathcal{I}_e$	SI/NA
	$\mathcal{V}_e$ [L]	1.4
	$\mathcal{T}_e$ [Nm]	130
	$\mathcal{P}_e$ [kW]	60
Battery	$\mathcal{I}_b$	HP
	$\mathcal{Q}_b$ [Ah]	31
	$\mathcal{K}_b$	60
Electric Motor	$\mathcal{I}_m$	PMSM
	$\mathcal{T}_m$ [Nm]	36
	$\mathcal{P}_m$ [kW]	38
Drivetrain	$\mathcal{I}_t$	MT-5
	$\mathcal{R}_{fd}$	3.7

Table 4.8 – Main features of investigated parallel hybrid-electric vehicle.

Results and Analysis

Fig. 4.11 illustrates the minimal energy consumption evaluated via various minimization methods over NEDC based on different powertrain component models. The black, blue, and cyan bars correspondingly represent the evaluations based on grid-point data, descriptive analytic models, and predictive ones.

The main errors were from SHM and GRAB-ECO with powertrain components models in terms of grid-point data. In fact, the minimal energy consumption via SHM is not strictly based on powertrain model of grid-point data due to the analytic nature of Hamiltonian function. As for GRAB-ECO with powertrain model of grid-point data, the error may be caused by the discretization level of driving cycle, and the non-strict fulfillment of final state of charge of the battery.

Detailed figures of the relative errors of minimal energy consumption are summarized in Table 4.9. In summary, both SHM and GRAB-ECO can evaluate the minimal energy consumption for parallel HEVs. Predictive analytic models of powertrain components were able to provide very similar minimal energy consumption for parallel HEVs compared with powertrain model of grid-point data.

The computation time of each evaluation is listed in Table 4.10 in terms of CPU time

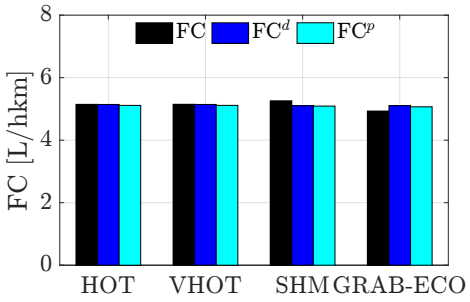

Figure 4.11 – Minimal energy consumption of reference parallel HEV over NEDC.

	HOT	VHOT	SHM	GRAB-ECO
ε^d[%]	-0.06	-0.10	-3.01	3.49
ε^p[%]	-0.63	-0.67	-3.22	2.78

Table 4.9 – Relative errors of minimal fuel consumption over NEDC.

in [s]. Significant computation time abatement was achieved by GRAB-ECO through shrinking the dimensions of control space.

Specifically, SHM minimized energy consumption within hundred of milliseconds, which was about threes times less than that of VHOT. Moreover, GRAB-ECO approximated the minimal energy consumption with eight to thirteen milliseconds, which was about ten times less than that of SHM.

	HOT	VHOT	SHM	GRAB-ECO
t_c^g [s]	204.78	0.2759	0.0928	0.0135
t_c^d [s]	224.82	0.3263	0.0912	0.0083
t_c^p [s]	224.46	0.2722	0.0918	0.0081

Table 4.10 – Comparison of average computation time over NEDC.

In addition to NEDC, the reference parallel HEV is investigated over FTP-72 and HYWFET. The minimal energy consumption are depicted in Fig. 4.10. Regardless of missions, the minimal energy consumption obtained through different optimal control techniques but with the same powertrain model typology was close to each other.

Exact errors of the minimal energy consumption are summarized in Table 4.11 and 4.12 for FTP-72 and HYWFET, respectively. The largest one was less than 4%.

The average computation time of evaluations is separately listed in Table 4.13 and 4.14 for FTP-72 and HYWFET. Apart from the significant abatement of computation

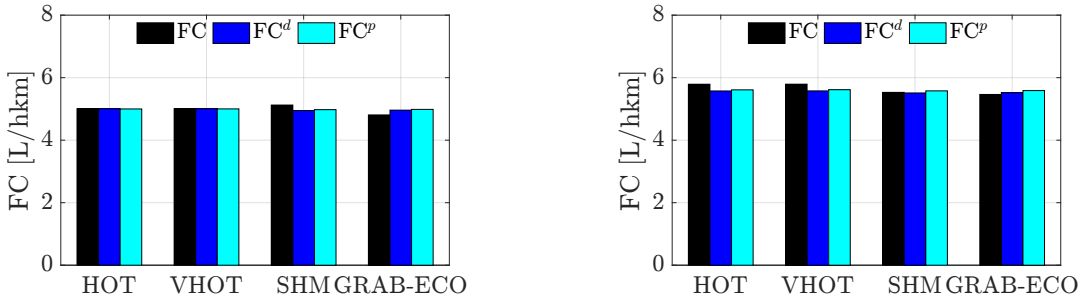

(a) FTP–72

(b) HYWFET

Figure 4.12 – Minimal energy consumption of reference parallel HEV over FTP-72 and HYWFET.

	HOT	VHOT	SHM	GRAB-ECO
ε^d [%]	0.01	0.01	-3.42	3.17
ε^p [%]	-0.12	-0.10	-2.88	3.69

Table 4.11 – Relative error of fuel consumption over FTP-72.

	HOT	VHOT	SHM	GRAB-ECO
ε^d [%]	-3.71	-3.69	-0.33	1.02
ε^p [%]	-3.10	-3.04	0.87	2.27

Table 4.12 – Relative errors of minimal fuel consumption over HYWFET.

time of SHM and GRAB-ECO, the average computation time was mission-dependent as well. This dependency was significant to HOT, VHOT, and SHM, except for GRAB-ECO.

	HOT	VHOT	SHM	GRAB-ECO
t_c^g [s]	221.84	0.3143	0.1056	0.0138
t_c^d [s]	262.14	0.3071	0.1041	0.0085
t_c^p [s]	285.07	0.3254	0.1056	0.0082

Table 4.13 – Comparison of average computation time over FTP-72.

	HOT	VHOT	SHM	GRAB-ECO
t_c^g [s]	243.23	0.1896	0.0656	0.0132
t_c^d [s]	187.30	0.1887	0.0638	0.0091
t_c^p [s]	186.82	0.1915	0.0648	0.0080

Table 4.14 – Comparison of average computation time over HYWFET.

To summarize, the average computation time of energy consumption minimization was gradually diminished from hundreds of seconds via HOT, to a few hundreds of milliseconds via VHOT, to about hundred of milliseconds through SHM, finally to about ten of milliseconds through GRAB-ECO. Meanwhile, the accuracy of minimal energy consumption was maintained at the same level.